Enhancement of thermal and mechanical stabilities of silicon doped titanium nitride coating by manipulation of sputtering conditions

Ehsan Mohammadpour[1], Willey Yun Hsien Liew[2*], Nicholas Mondinos[1], Mohammednoor Altarawneh[3], Sunghwan Lee[4], Nik Radevski[1], Manickam Minakshi[5], Amun Amri[6], Hong Ngee Lim[7], Zhong-Tao Jiang[1*],

[1]Surface Analysis and Materials Engineering Research Group, College of Science, Health, Engineering and Education, Murdoch University, Murdoch, WA 6150, Australia
[2]Faculty of Engineering, Universiti Malaysia Sabah, Jalan UMS, 88400, Kota Kinabalu, Sabah, Malaysia
[3]Department of Chemical and Petroleum Engineering, United Arab Emirates University, Sheikh Khalifa bin Zayed Street, Al-Ain 15551, United Arab Emirates.
[4]School of Engineering Technology, Purdue University, West Lafayette, IN 47907, United States
[5]College of Science, Health, Engineering and Education, Murdoch University, Murdoch, WA 6150, Australia
[6]Department of Chemical Engineering, Universitas Riau, Pekanbaru 28293, Indonesia
[7]Department of Chemistry, Faculty of Science, University Putra Malaysia, 43400 UPM Serdang, Selangor, Malaysia

*Corresponding author: Willey Yun Hsien Liew (wyhliew@ums.edu.my) and Zhong-Tao Jiang (Z.Jiang@murdoch.edu.au)

Keywords: synchrotron radiation; thermal stability; mechanical properties; oxidation; bias voltage; TiSiN

Highlights

- Substrate bias voltage influences on the structure and mechanical properties of Si doped TiN_x coatings up to 800 °C.

- Microstructural and phase thermal stability of TiSiN coatings

- 50% increase in Hardness and Young's modulus of the coatings from bias voltage increase.

- Si dopants improve oxidation resistance of TiSiN coatings with a reduced oxidation rate.

Abstract

This study investigates the influence of substrate (AISI M42 tool steel) bias voltage (from -30 V to -80 V), on the mechanical properties of magnetron sputtered TiSiN coating derived from Ti and Si targets. Thermal stability, microstructure (crystallite size, microstrain, lattice constant), morphology and mechanical (hardness, Young's modulus, residual stresses) properties, of the deposited TiSiN coatings, were investigated with synchrotron powered X-ray diffraction (SR-XRD), X-ray photoelectron spectroscopy, field emission scanning electron microscopy, and nanoindentation techniques. Rietveld analysis, of the *in-situ* SR-XRD, in the temperature range of 25-800 °C, demonstrated cubic TiN form in (Ti,Si)N solid solutions, with TiO_2 and Ti_2O_3 identified at lower bias voltages. Density functional theory supplemented the experimental results.

Increase in the bias voltage resulted in: (i) a decrease in Si content, (ii) significant smoothening of surface morphology, (iii) change in the phase composition and microstructure, (iv) improved oxidation resistance and thermal oxidation threshold, and (v) hardness and Young's modulus of the coatings increased up to 50% to 33 GPa and 450 GPa, respectively.

1. Introduction

Modern machining tools, such as: cutting tools, drills, hobs, mills, and machining inserts; seek new coating materials that resist wear, fatigue or crack propagations of those tools. Hard coatings can be applied to improve the efficiency and mechanical properties of these engineering tools. Transition metal nitride hard coatings have greatly improved machining performance of high-speed cutting, stamping and moulding tools. Among them, TiSiN coatings exhibited outstanding properties, such as: high hardness, good wear resistance [1], and good thermal and chemical stability [2]. These properties are thanks to its nanocomposite microstructure, consisting of TiN nanocrystals (nc-) embedded in an amorphous (a-) Si_3N_4 matrix (nc-TiN/a-Si_3N_4) [3]. The maximum improvement in mechanical properties, of TiSiN systems, is expected when the extremely fine nc-TiN crystals (∼3 nm) are surrounded by a-Si_3N_4, at a Si content of ∼7 at.% [4].

Sophisticated metal nitride coatings can only be achieved by an appropriate choice and precise control over the parameters governing the sputter deposition process. Deposition parameters, such as: Si targets current, substrate negative bias voltage, temperature, pressure and nitrogen flowrates [5],[6],[7]; are the most important factors that determine the Si content, microstructure, bonding and crystalline structure, deposition rate, surface roughness, and mechanical properties of the sputtered coatings [8]. Substrate bias voltage has a significant influence on the atom mobility, on the coating surface, and ion bombardment during sputtering [9],[10].

Benegra *et al.* [11] showed that TiN coating exhibited higher compressive residual stress and lower average grain sizes, when the negative bias voltage increases from 0 to -100 V. Early studies of Vaz *et al.* [12] confirmed the formation of TiN nanocrystals and substation, of Ti atoms, by smaller Si atoms in TiSiN coating, during ion-bombardment. It was shown that the mechanical properties of coating films could be optimised by adjusting the negative bias voltage [13],[14],[15]. Applying a

proper bias voltage to the substrate can significantly improve the ionisation and energy of the sputtered particles, and enhance the films crystallisation [16],[11]. The decrease in deposition rate, with an increase of the substrate bias voltage, would be related to the resputtering phenomena and densification of the coating; which is due to strong collision energies of the ions. Choi *et al.* [9] showed that in the Ti-Si-N coating system the deposition rate and Si contents decrease as the substrate bias voltage increases from 0 to -500 V and significantly influenced the mechanical properties of the coatings. Chang *et al.* [17] showed that in TiSiN coatings, the combination of ion-bombardment, Si alloying and re-sputtering, at higher bias voltages, formed nanocomposite structure and increased the coating hardness and elastic modulus up to 35 and 360 GPa, respectively. Cheng *et al.* [8] showed that the increasing Si content of the TiSiN coating to 7 at.% progressively reduces the TiN crystallite size and at the same time increases the coating internal stresses. Wo *et al.* [7] studied the mechanical properties of multilayered TiN/TiSiN coatings and concluded that the relative thickness of layers determines the hardness and deformation mechanisms of the coatings. Coatings with thicker TiSiN layers showed higher hardness and deformed by the crack prorogation mechanism. Yazdi *et al.* [2] studied the TiSiN coatings, with various Si concentrations, before and after annealing in air, and showed that it is possible to reduce the nc-TiN crystal sizes to ~ 6 nm. This was achieved by adjusting the Si content and enhanced the hardness to 40 GPa. His results suggest that adding Si improved the oxidation resistance at 700 °C, however, the hardness of the coatings almost reduced by half 2 hours after annealing. Greczynski *et al.* [18] showed that the deposition technique has direct influences on the nanostructure, nanochemistry and mechanical properties of TiSiN coatings deposited by hybrid high-power pulsed/dc magnetron (HIPIMS/DCMS) co-sputtering system.

Although there are comprehensive studies on the nanostructure and mechanical properties of TiSiN coatings, studies on the thermal stability and oxidation resistance of these coatings are rather limited. In this study, the influence of substrate bias voltage, on the structure and mechanical properties of TiSiN nanocomposites, was investigated using high-resolution SR-XRD beamline, in the temperature range 25 to 800 °C. The results provide precise microstructural and phase composition data, which enhances the fundamental understanding of the effect of Si dopants, on the thermal stability of TiSiN coatings. First principle density functional theory (DFT) calculations were employed to study the effect of bias voltage and Si content, on the thermal expansion of TiSiN coatings. Combination of Rietveld refinement analysis, nanoindentation data, x-ray photoelectron spectroscopy, and field-emission electron microscopy imaging showed that optimised bias voltage could enhance the mechanical properties of the TiSiN coatings significantly.

2. **Experimental**

2.1. Thin film coating preparation

The TiSiN hard coatings (9 samples) were deposited onto AISI M42 tool steel substrates (hardened to HRC 62). A closed-field unbalanced magnetron sputtering system, with a four-target configuration, was used. The steel substrates were finely polished (R_a ~0.02 μm), degreased, ultrasonically cleaned, and subsequently blown dry in flowing nitrogen gas. The magnetron sputtering system comprised of three Ti targets (purity > 99.7 at %) and one Si target (purity > 99.9 at %). The size of the targets was 380 mm × 175 mm × 8 mm. The coating equipment had a rotating substrate holder; a speed of 10 rpm was used to permit a homogeneous composition of the

coatings. The target-to-substrate distance was 17 cm. The vacuum chamber was pumped down to a background pressure less than 2×10^{-6} Torr before deposition. After that, the Ar working gas (purity 99.995 at %) pressure was set at ~1.3×10^{-3} Torr by controlling the flow rate (50 sccm) of Ar *via* an MKS mass flow controller. The DC current, applied to each Ti target, was fixed at 8.0 A (~2.3 kW for each Ti target), while the target current to the Si target was 2.5 A (sputtering power ~0.8 kW). The nitrogen content in the coatings was controlled using a closed-loop optical emission monitor (OEM), with a setting at 60 %, which regulated dynamically the flow of N_2 reactive gas (purity 99.995 at %) *via* a fast-responding piezoelectric valve. The sputter working pressure, with Ar/N_2 mixed gases, was maintained at 2×10^{-3} Torr. The deposition process, of the hard coatings, comprised three major steps: plasma ion cleaning, Ti adhesive layer (0.2 μm), TiN buffer layer (0.4 μm), $TiSi_xN$ compositional gradient layer (0.3 μm), and TiSiN top layer (2 μm). The Si content in the compositional gradient layer was increased linearly, in the thickness direction, in order to accommodate the internal stress. The substrate holder was heated by a radiation heater (5 kW), located in the centre of the vacuum chamber, and the substrate temperature was maintained at 550 ºC during deposition. The ion etching, of the steel substrates, at the first stage at -600 V, was employed for 30 min to remove the oxide layers on the substrate surface. For the sputter deposition of Ti (10 min), TiN (30 min), and $TiSi_xN$ (20 min) layers; the bias voltage was reduced to -60 V. The top TiSiN layer was the deposited for 120 min. The substrate bias was operated in a pulsed mode, at a frequency of 250 kHz. In this case, in order to study the effect of bias voltage, different bias voltages (from -30 V to -80 V) were applied to the substrate holder, when the TiSiN top layer (2 μm) was coated. The bias voltage mainly determined the energy of ions, bombarding the growing surface. For comparison, a binary TiN coating of similar total thickness was prepared, at a bias voltage of -50 V (Sample No. 532A).

2.2. *In situ* SR-XRD characterisations

In situ SR-XRD experiments were performed on the Powder Diffraction beamline, at the Australian Synchrotron, with monochromatic X-rays, $\lambda = 0.827$ Å, and verified with the standard reference material (LaB6 660b), as supplied by the USA National Institute of Standards and Technology (NIST). The incidence angles of the X-ray beam (ω) were in the range of 4.1° to 5.9°. The diffraction data was collected by a Mythen microstrip detector, over the range of $10° \leq 2\theta \leq 89°$, in the flat-plate asymmetric reflection geometry. The coated substrates were mounted on a Pt heating stage, in an Anton Paar HTK-2000 high temperature furnace, and aligned to the centre of rotation on the diffractometer. The heating rate was 10 °C/min, from ambient temperature up to 700 °C, in air atmosphere. The temperature difference between the sample surface and Anton Parr furnace was calibrated manually before the *in situ* experiments were carried out. Diffraction patterns of 6 samples (bias voltages of -30, -40, -50, -60, -70 and -80 V) were obtained at three temperatures (25, 200 and 500 °C) below, and three temperatures (600, 700 and 800 °C) above the deposition temperature of 550 °C; this was due to time constraints, at the synchrotron facilities. Each data acquisition time, at designated temperature, was 120 s.

The diffraction patterns were analysed with the TOPAS v5 academic software [19] with the Rietveld method [20]. The atomic positions for the structural models, based on the main identified phases of the coating, were extracted from the Crystallography Open Database [21]. Modelled peak shapes were used to determine the volume-weighted mean crystallite sizes (L_{vol}) and microstrain (e_0). An accurate description of the peak shapes, in all of the diffraction patterns, was obtained by applying correctional functions, for a flat plate, in a fixed incident beam geometry [22]–[24]. The initial parameters for the refinement, as well as phase determination, were obtained from the JCPDS cards. All the diffraction patterns shown in Figures S1 to S7 of the supplementary section were

analysed by Rietveld refinement method. Figure 1 is representative of the diffraction patterns from refinement results. It shows the pattern for TiN sample at 800 °C, which contains peaks from the substrate (Fe and FeWC), and coating (TiN, TiO_2) phases.

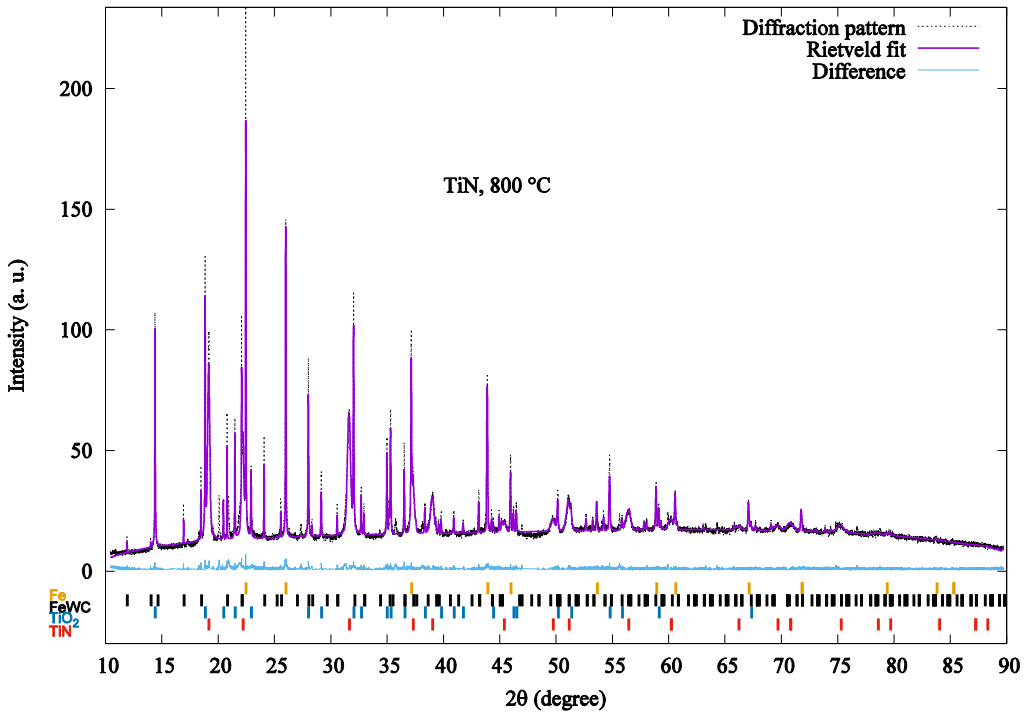

Figure 1. Experimental SR-XRD and Rietveld refinement profile of TiN coating at 800 °C. The *hkl* values for each phase are indicated by the small vertical bars.

2.3. Surface analysis

Surface morphology of the thin film coatings was inspected with a field emission scanning electron microscope (FESEM) (Zeiss Neon 40EsB), coupled with Energy-dispersive X-ray spectroscopy (EDS). FESEM images were obtained with InLens detectors, at various magnifications, at 5 kV, and a working distance of ~2.4 mm. X-ray photoelectron spectroscopy (XPS) analysis provided comprehensive information on the chemical state, bonding structure and elemental composition of

the outermost layers of surfaces. XPS data of all thin films was acquired with a Kratos Axis Ultra XPS spectrometer (Kratos, Manchester, UK). An Al-Kα monochromatic radiation (hv = 1486.6 eV) source and at an operating current of ~10 mA and voltage of ~15 kV, was used. The XPS machine was also equipped with a cold stage and an Ar ion gun, for etching and depth profiling. The samples were mounted on a steel sample holder. The chamber pressure was reduced to 2.9×10^{-9} Torr and maintained at that level for the analysis. XPS survey spectra were acquired from both etched (6 minutes of ion sputtering) and unetched samples. High resolution XPS spectra were recorded immediately after 6 minutes, of the Ar^{+} sputtering. Etching was done to remove any surface oxide layers and to reduce the Ti^{4+} ions, in order to lower oxidation states. Pass energy of 20 eV was used for high resolution Si*2p* and N*1s* photoelectron lines measurement. CASA XPS (Version 2.3.18) software was used for processing and fitting the peaks of the XPS spectra.

2.4. Nanoindentation measurements

Nanoindentation data was collected, to study the mechanical properties of the samples. An Ultra-Micro Indentation System 2000 workstation (CSIRO, Sydney, Australia) was used, together with a diamond Berkovich indenter. The calibration of the area function, of the indenter tip, was carried out with a standard fused silica specimen. Load control method was employed, in which the loading was increased in 20 steps to reach the pre-defined maximum loading, then it was decreased in 15 steps to zero. For each of the steps, the displacement was recorded. The maximum loading was defined as 8 mN, which was based on the considerations that the maximum displacement, during indentation, should be no higher than 10% of the coating thickness, and that high loading may result in micro-cracks, in the coating, which was thought to be relatively brittle, compared with metal coatings.

2.5. DFT computational simulations

All structural optimisations and calculations were performed with the generalised gradient approximations (GGA), with the PW91 functional [25], as implemented in the VASP package [26]. Energy cut-off for plane waves included in the expansion of wave functions was 500 eV. Pseudo-atomic calculations were performed for Ti: $3d^5 4s^1$ and N $2s^2 2p^3$. *k*-point sampling, for reciprocal space integration, was optimised and a 21×21×21 Gamma scheme, for cubic structures, was adopted. The thermodynamic properties of TiN phase were explored with the quasi-harmonic Debye–Slater model, as implemented in the Gibbs2 code [27]. In all temperature dependent property calculations, the Vinet's equation of state was adopted to fit the energy–volume curves [28]. To calculate the elastic constants and determine the second derivatives, we used a finite differences method as implemented in VASP package (IBRION=6).

3. Results and Discussions

3.1. Microstructure and chemistry

Surface quantitative elemental concentrations, in the TiSiN coatings, from high resolution XPS, are listed as a function of sputter substrate bias voltage in Table 1. As the bias voltage changes from -30 to -80 V: (1) Ti changes from 31.4 to 41.8 at%; (2) Si from 5.1 to 0 at%; (3) N from 23.5 to 39.5 at%. The changes in the Si content can be attributed to the different acceleration effects, of the bias voltage, on the Si ions, which are lighter than Ti ions. Si ions accelerate faster than Ti ions, when the bias voltage and energy level is relatively low. As the bias voltage increases to -70 and -80 V, the Si content of the coatings drops to zero, which could be caused by two main reasons: (1) After the Ti ions reach a sufficiently high energy level, whilst being accelerated toward the

substrate, at higher substrate voltages, the Ti concentration will suppress Si content within the coatings, (2) heavy Ti ions, with high kinetic energies, may re-sputter the lighter Si adatoms near the surface of the substrate, as reported in similar studies on TiSiN and TiAlN systems.

Table 1. Elemental compositions of TiN and TiSiN unbalanced magnetron sputtered coatings, deposited at different bias voltages, acquired *via* XPS survey scans.

Sample's name	**Atomic percentages of the elements (at %)**					
	Bias voltage (V)	Ti	Si	N	C	O
TiN	-	41.73	-	37.67	1.12	19.48
TiSiN	-30	31.40	5.09	23.47	4.67	35.37
	-40	34.43	6.22	28.80	2.81	27.75
	-50	36.53	4.09	34.31	1.19	23.88
	-60	39.40	4.32	36.94	-	19.33
	-70	40.89	-	38.86	-	20.25
	-80	41.83	-	39.45	-	18.71

Figure 2 shows the SR-XRD patterns, as a function of the substrate bias voltage, for as-deposited samples. The diffraction patterns show that the TiN and TiSiN coatings consist of TiN phase, in the B1 type (fcc crystal) structure, with space group Fm-3m. List of detected diffraction peaks, of TiN and diffraction angles, are shown in Table S1. SR-XRD data, of the samples in the studied temperature range, are shown in Figures S2 to S7, of the supplementary information. All of the coatings exhibited strong texture along TiN(111), which is more pronounced in TiSiN-60V. TiN

(200) is convoluted by the peak caused by the substrate. Rietveld Refinement results suggest that TiSiN-30V and TiSiN-40V coatings consist of two TiN phases: a nanocrystal TiN phase, with a lattice constant of 4.24 Å, and a TiN phase, with very coarse grains, which has a slightly smaller lattice constant of 4.23 Å. SR-XRD data shows no evidence of crystalline Si_3N_4 or Ti-silicide phases.

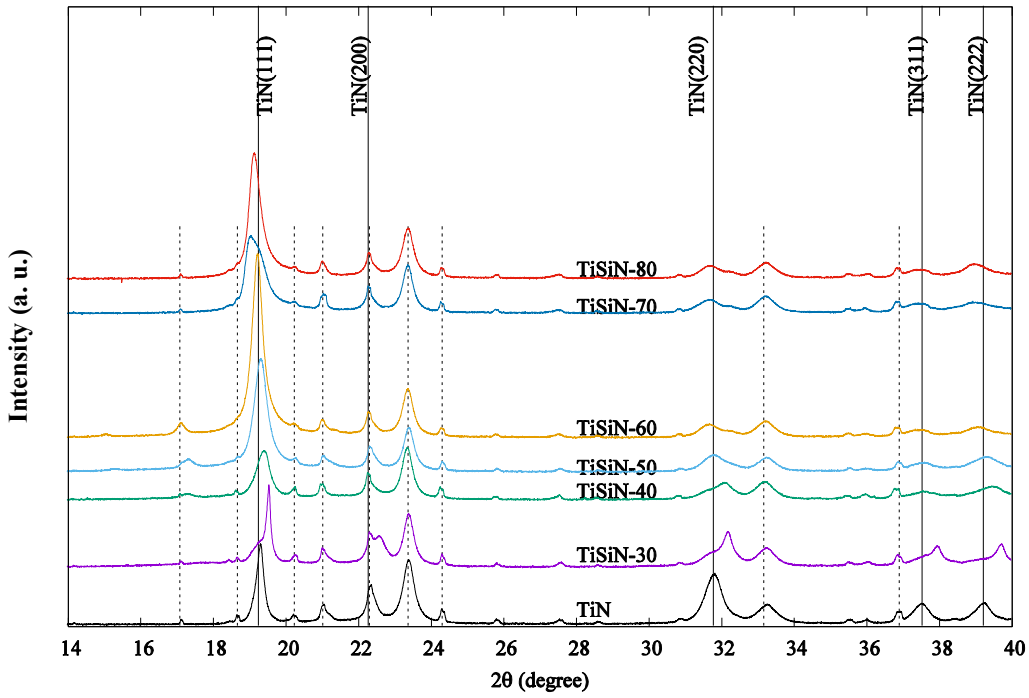

Figure 2. SR-XRD patterns of the as-deposited TiSiN coatings, at varying bias voltages, at room temperature. The dashed vertical lines indicate substrate peaks.

Figure 3 shows the XPS spectra, of Si 2p and N 1s for Ti-Si-N coatings. The Si 2p showed two peaks, with binding energies of 99.0 and 101.4 eV, corresponding to the Si and silicon nitride

phases, respectively. N 1s spectrum can be fitted by two peaks, located at 397.0 (main peak) and 399.5 eV (satellite peak), corresponding to TiN and Si_3N_4 phases. The absence of Si_3N_4 diffraction peaks, in SR-XRD results, suggests that this phase exists in amorphous form. The combination of this evidence supports the findings from the structural analysis; that the TiSiN films consist of crystals TiN embedded in an amorphous Si_3N_4 matrix, which was observed in TEM studies on Ti-Si-N systems [17].

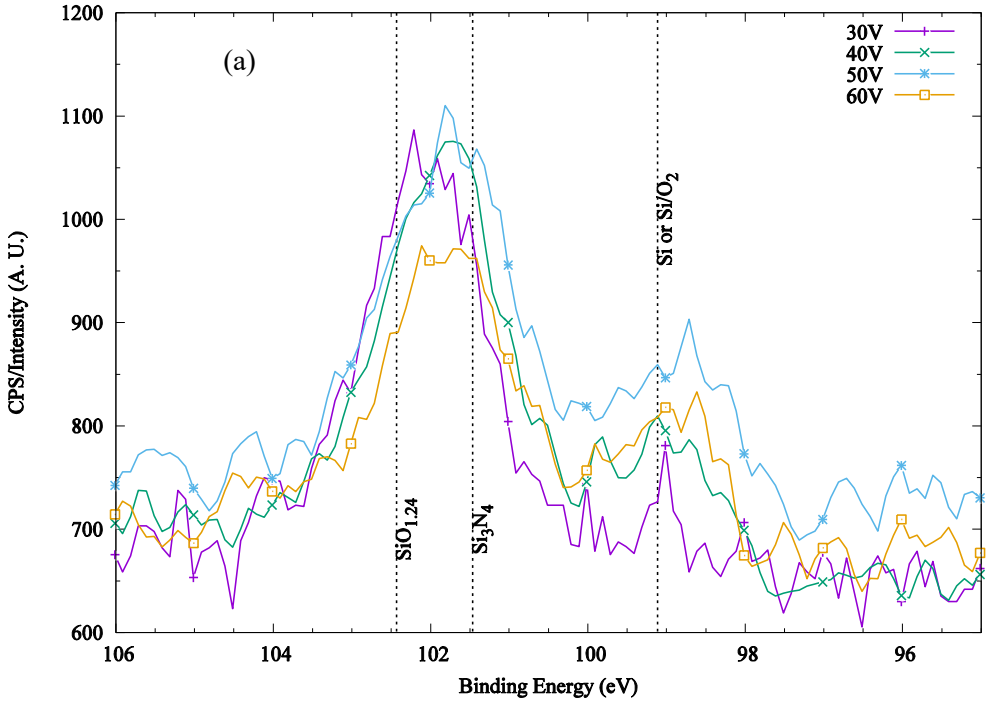

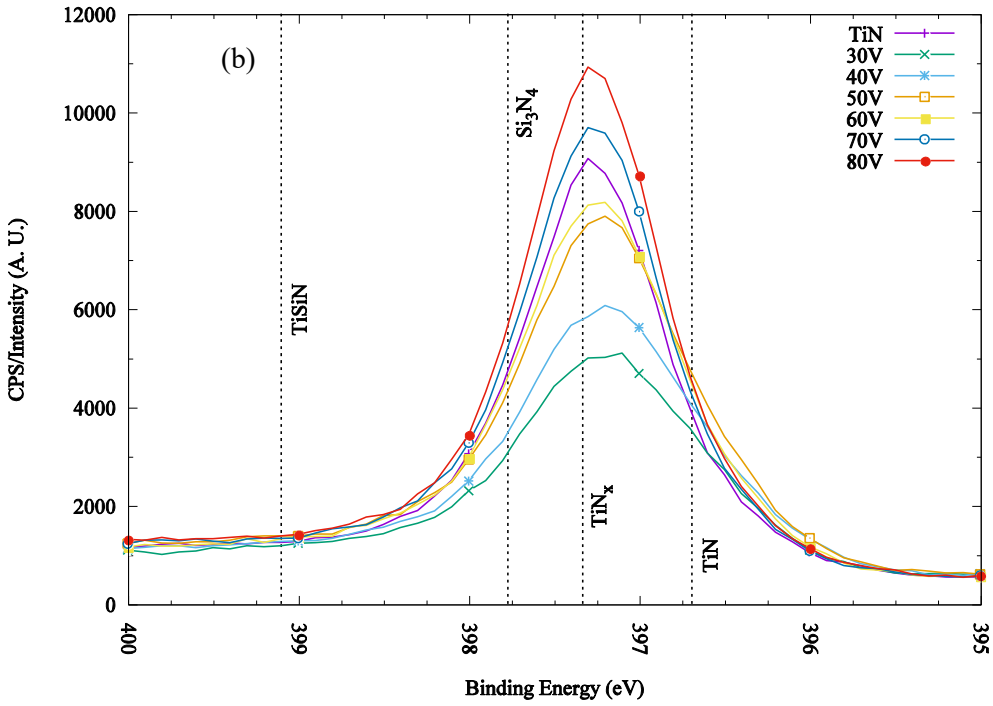

Figure 3. (a) Si 2p and (b) N 1s XPS diffractograms of sputtered TiSiN coatings deposited at various bias voltages.

Figure 4 shows the SR-XRD patterns, of TiSiN coatings, at 800 °C. Crystalline tetragonal TiO_2, in P42/mnm space group was detected in TiN, TiSiN-30 and TiSiN-40 coatings. The lattice constant of TiO_2 was measured as a = 4.623±5% Å and c = 2.983±5% Å. Rhombohedra Ti_2O_3 (space group R-3c) was only identified in TiSiN-40 above 700 °C, with lattice constants of a = 5.14±10% Å and c = 13.65±10% Å. The evolution of TiO_2 and Ti_2O_3 phases, in different samples during the *in-situ* experiments, are illustrated in Figures S1 to S7 of the supplementary section. TiO_2 peaks were observed in the SR-XRD pattern of TiN sample at 600 °C, while the coatings with Si dopants only showed TiO_2 at 700 °C. The observed formation of the TiO_2 layer, on top of TiN coatings, could be resulted from outward diffusion and oxidation of Ti due to poor oxidation

resistance, of pure TiN coatings, at high temperatures. It is interesting to note that the quantitative SR-XRD study shows that the TiO_2 amount detected, in TiSiN coatings, is lower than that in the TiN sample. These results suggest that Si dopants improved oxidation resistance of TiSiN coatings and reduced the oxidation rate, with the threshold of the oxidation temperature increased by about 100 °C. Coatings deposited, at bias voltages above 40 V, consist of the TiN phase up to 800 °C. Between 700 and 800 °C, a major phase transition in the steel substrate takes place, where Fe (Im-3m) transforms to Fe (Fm-3m).

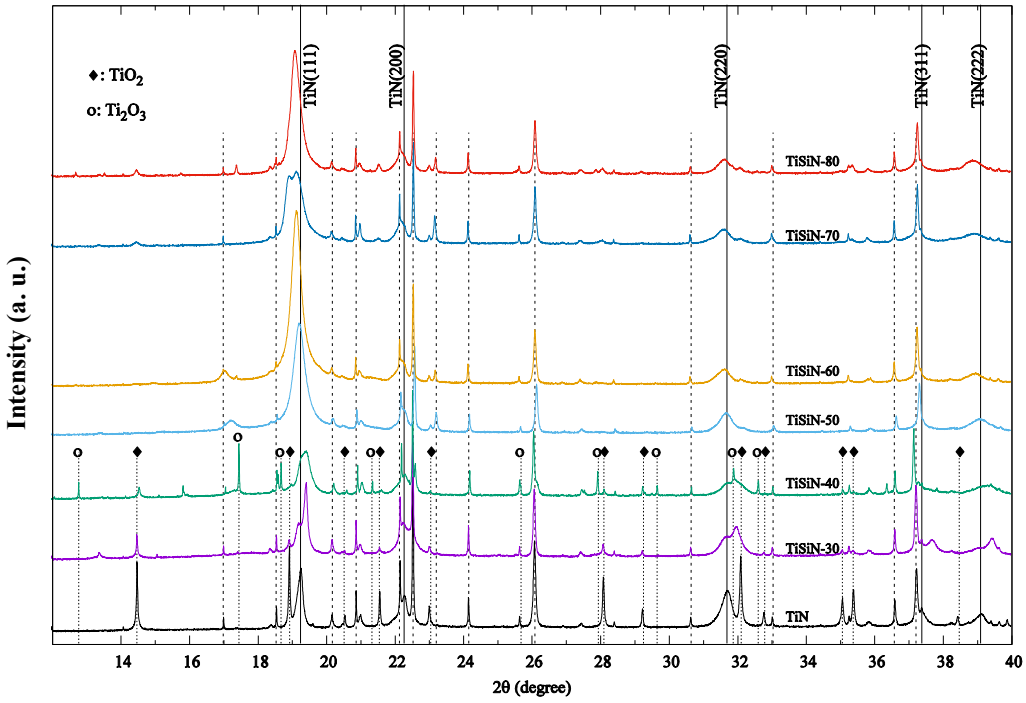

Figure 4. SR-XRD patterns of TiSiN coatings deposited at various bias voltages, measured at 800 °C. The dashed vertical lines indicate substrate peaks

Figure 5 shows the TiN lattice constant, as a function of temperature, from Rietveld refinement results. The lattice constant of TiN at room temperature ranged from 4.25 to 4.27 Å, which is slightly smaller than the reported value from Tkadletz experiment [29] and present QHA modelling predictions. Comprehensive studies on the changes in the TiN lattice constant, in Ti-Si-N coating systems, showed that incorporation of smaller Si atoms, in the position of Ti, leads to the formation of solid solutions in the form of (Ti,Si)N. TiSiN-30V shows the smallest lattice constant amongst all the samples, in this study, suggesting the highest Si incorporation into the TiN lattice, which is in agreement with the higher Si content of this coating concluded from Table 1. The TiN lattice constant increased consistently, as the Si content of the coatings decreased, and the TiSiN-80V sample showed the largest lattice constant. This evidence confirms the formation of (Ti,Si)N solid solutions, with various Si contents, in TiSiN coatings. The TiN lattice constant measurements, based on SR-XRD data, showed a gradual expansion of the lattice constants, with the increase of the negative bias voltage. Thermal expansion, during annealing, also leads to expansion of lattice constants, as confirmed by the experimental results, on the TiN powders; as conducted by Tkadletz *et al* [29] and Bartosik *et al.* [30]. The accuracy of the QHA modelling, for bulk TiN, could be estimated when it is compared to experimental results of Bartosik *et al.* [30], on powdered TiN. There is a small mismatch (< 2%) between QHA predictions and results from SR-XRD experiment, especially at higher temperatures. This mismatch could be due to: (1) differences in thermal expansion coefficient of M2 steel and thin film coatings, and (2) Si dopants incorporated in TiN lattice. The TiN lattice constant measured for samples deposited, with the bias voltage of -80 V, is very close to the modelling results, which could be due to the absence of Si (refer to Table 1).

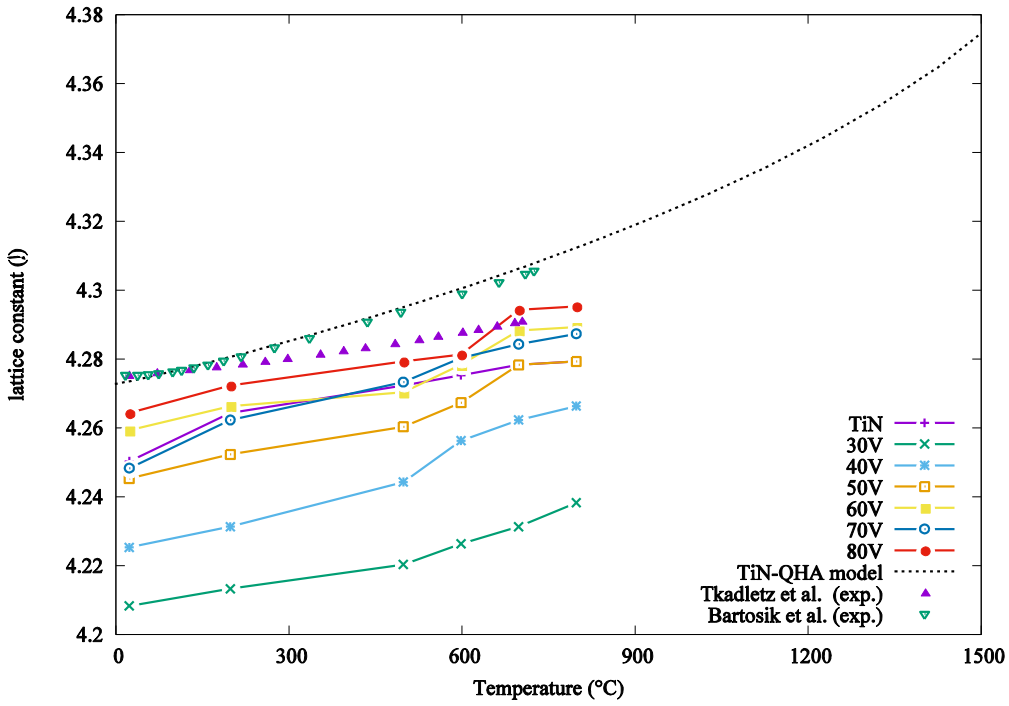

Figure 5. Experimental TiN lattice constants in TiSiN coatings deposited at various bias voltages and temperatures, including theoretical prediction.

Figure 6 schematically summarises the phase evolution, in TiSiN coatings, during the *in-situ* experiments, within the temperature range 25 to 800 °C. Ti oxides, such as: TiO_2 and Ti_2O_3 – were observed only in coatings deposited, at low bias voltages; while coatings deposited at higher bias voltages (> 40 V) consist of only cubic (c-) (Ti,Si)N solid solutions. TiO_2 was observed in 3 of the coatings, at temperatures higher than 600 °C, and Ti_2O_3 only detected in TiSiN-40V above 700 °C.

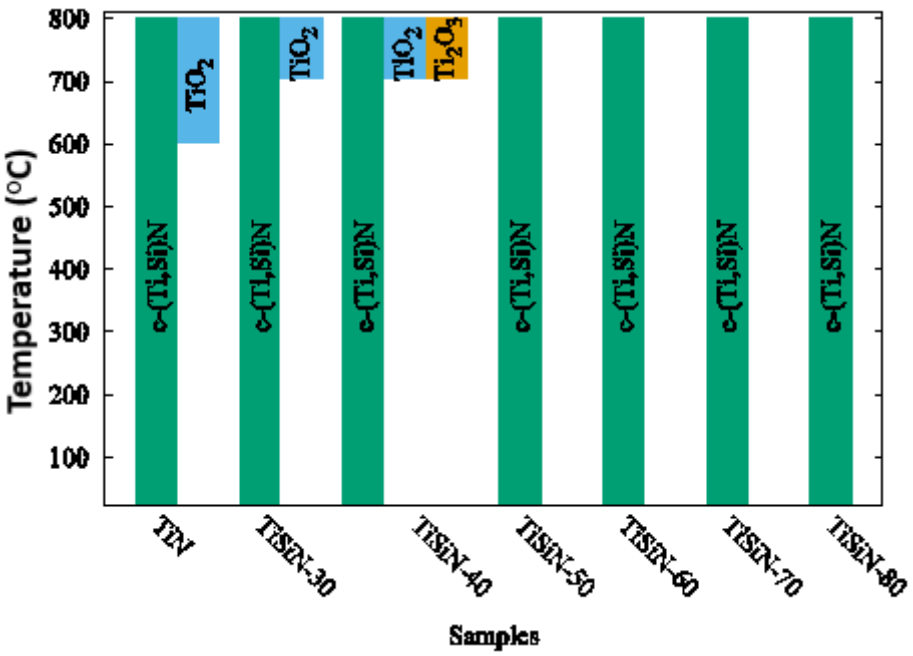

Figure 6. Schematic summary of the phase evolution for TiSiN coatings obtained from the *in situ* experiment analysis.

Figure 7 shows the effect of measurement temperature, on the crystallite size and microstrain of TiN crystals, in TiSiN coatings. Results show that as-deposited TiSiN-30V coating possesses the smallest crystallite size of 10 nm in co-existence with the coarse TiN phase. The as-deposited TiN crystallite size increased almost monotonously, from 10 to 35 nm, as the bias voltage increased, from -30 to -80 V. TiSiN-50V is the only exception – exhibiting 17 nm TiN nanocrystals, which is slightly lower than 20nm TiN crystals, in the TiSiN-40V coating. These coatings showed excellent resistance to crystallite growth during the *in-situ* experiments at lower temperatures (< 500 °C). TiN coating showed a sharp increase in crystallite growth rate (≈ 33%) between 600 °C and 800 °C. TiSiN-30V showed the highest crystallite growth rate (≈ 70%), which started at 500° C. The crystallite size increased from 10 to 17 nm. The co-existence of two TiN phases, featuring

fine and coarse grains, may lead to unsuccessful nanostructure optimisation of the coating. TiSiN-40, -50 and -60V showed excellent crystal size stability (17-24 nm), within the studied temperature range. It could be due to the successful formation of a nanocomposite structure, of nc-TiN/a-Si_3N_4, which inhibits the diffusion processes and subsequently stopped the grain growth in these coatings. Coatings deposited with the highest bias voltages, TiSiN-70 and TiSiN-80, showed growth rates of less than 10%, between 500 and 800 °C. Figure 7(b) illustrates the microstrain evolution, of TiN crystals, as a function of experimental temperature. The result shows that the coatings deposited at lower bias voltages (TiSiN-40 and TiSiN-30) exhibit higher microstrain. The internal stress in the coatings decreases as the temperature increases, in all the coatings with different rates, which is likely attributed to the structural relaxations driven by the thermal energy involved. TiSiN-30 and TiN coating show the highest and lowest microstrain levels at 800 °C, respectively, while internal strain in TiSiN-60 reduced with the lowest rate compared to the rest of the coatings.

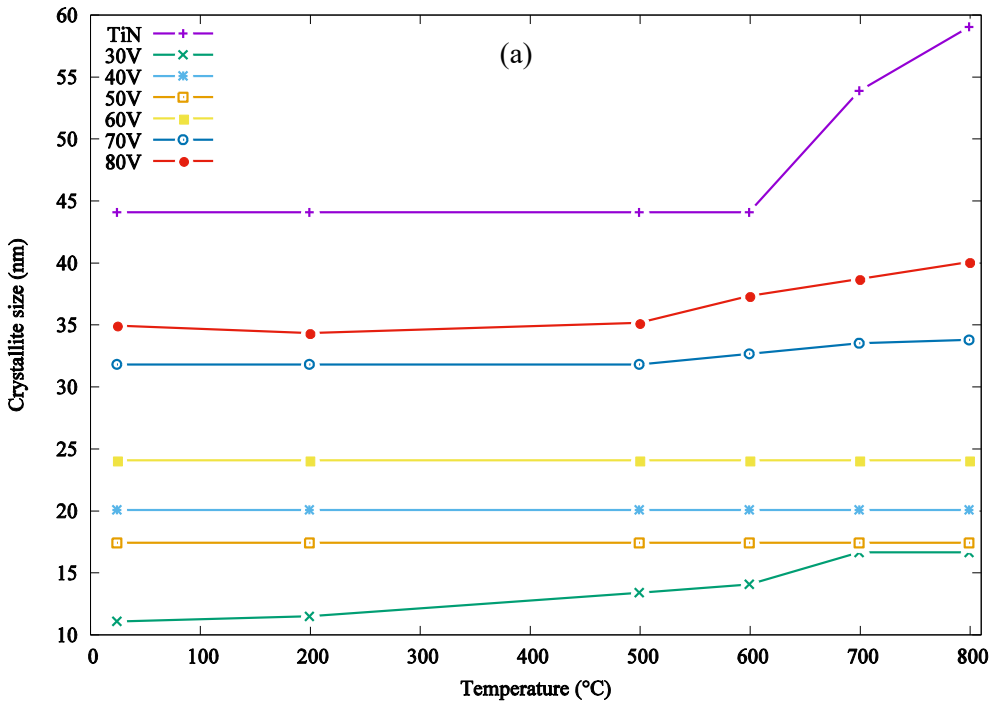

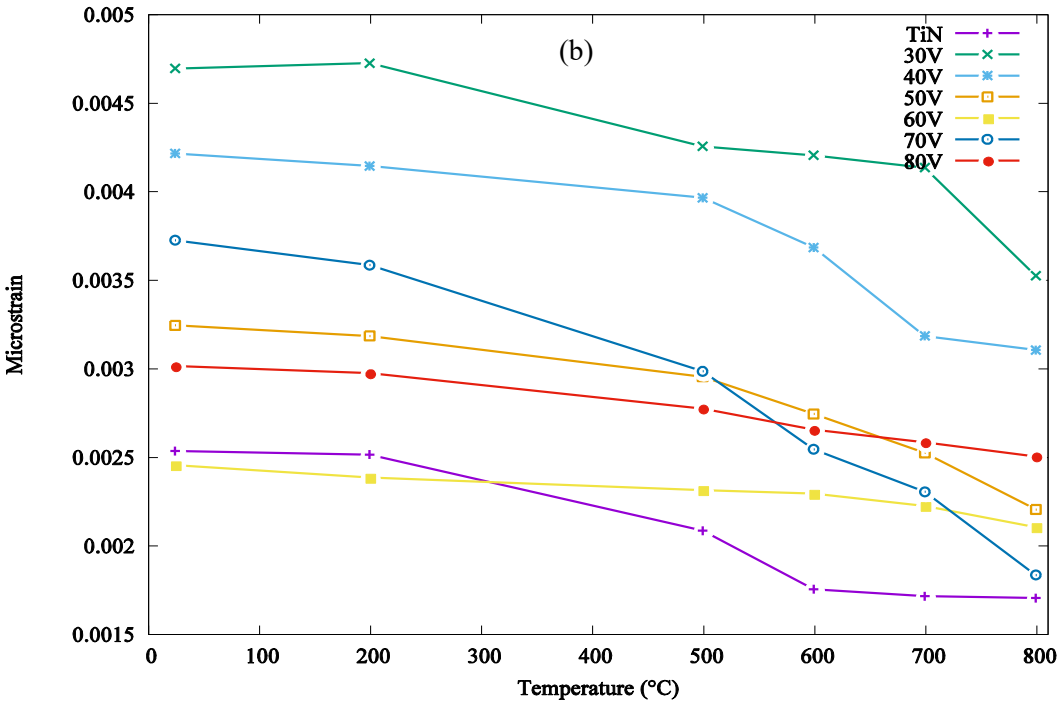

Figure 7. (a) crystallite size and (b) microstrain of TiN phase as a function of measurement temperature from *in-situ* experiments.

3.2. Surface morphology

The surface morphology of TiSiN coatings, deposited at various bias voltages, is shown in Figure 8. The coatings gradually became denser and smoother, at high bias voltages. This could be due to the high energy impinging ions from the higher plasma intensity of the two target energy sources; increasing the number of nucleation sites, resulting from the increasing defects. The (Ti,Si)N nanocrystalline were formed in island-shaped particles at lower bias voltages (*e.g.*, -30 V and -40 V) and TiN coatings. TiSiN-30V particularly showed a porous microstructure, consisting of sharp edged micro crystallites (50-100nm) conglomerating into globular structures of approximately 400-500 nm diameter. TiSiN-40V, on the other hand, had smoother cauliflower styled micro crystallites into the globular structures. These structures could be responsible for the

poor resistance, of these coatings, to oxidation at higher temperatures. This is indicated by the SR-XRD results. As the bias voltage increases, the (TiSi)N grains gradually diffuse and linked together (Figure 8d-e), and packed densely in TiSiN-50 and TiSiN-60 coatings. It seems that higher bias voltages assisted in producing smooth surfaces and uniform microstructures; as observed in TiSiN-60. The surface morphology of TiSiN-70 and TiSiN-80 again shows some features, which could be due to two simultaneous phenomena: (1) zero Si content and (2) very high energy ion bombardment during deposition. SR-XRD results confirm that all the coatings deposited at bias voltages > 40 V are thermally stable up to 800 °C, regardless of their Si content.

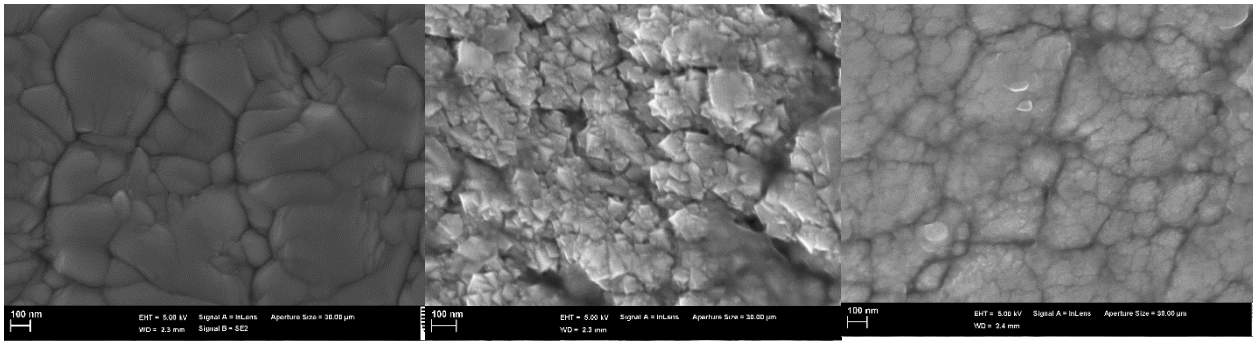

(a) TiN (b) TiSiN-30V (c) TiSiN-40V

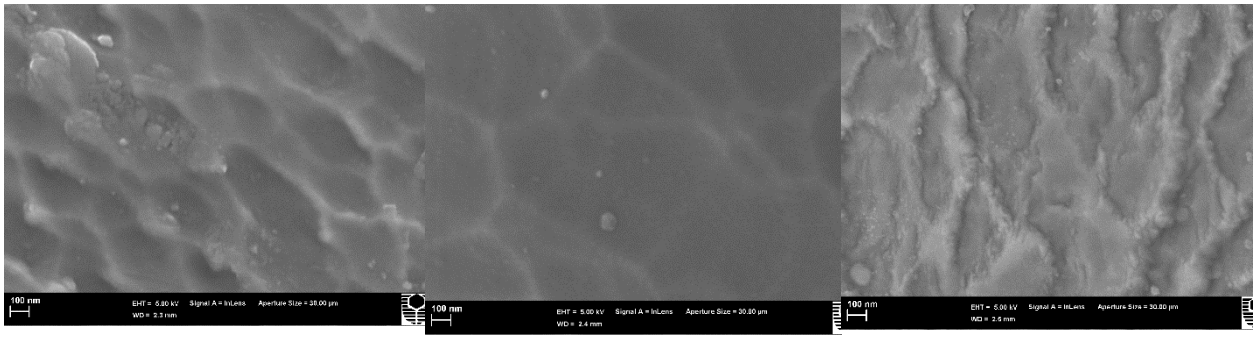

(d) TiSiN-50V (e) TiSiN-60V (f) TiSiN-70V

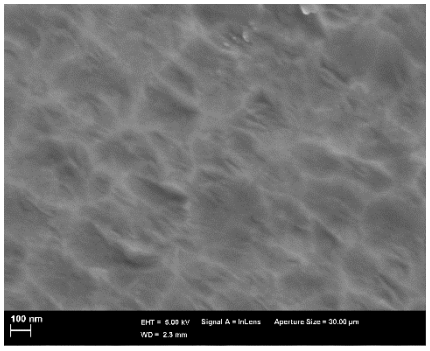

(g) TiSiN-80V

Figure 8. FESEM images of TiN and TiSiN coatings deposited at different bias voltages.

3.3. Mechanical properties

Nanoindentation results, of TiSiN samples, deposited at the various bias voltages, are shown in Figure 9 (It should be noted that 30 V also represents sample TiSiN-30V *etc*.). Coating hardness continuously improved, from 23 to 33 GPa, as the bias voltage increased from -30 to -80V. The elastic modulus, of the coatings, also increased from 300 to 440 GPa, as the bias voltage increased from -30 to -80V. Densification of the coatings and the higher residual stress, induced by ion bombardment, at higher bias voltages, which is due to the higher energy of the ions, can contribute to the higher hardness and the observed Young's modulus. Rietveld refinement and XPS results suggested that TiSiN-50 and TiSiN-60 coatings contain nanostructure c-(Ti,Si)N crystals, surrounded by amorphous Si_3N_4. FESEM images also showed that these samples, and TiSiN-70, TiSiN-80, exhibit low surface roughness with high density coating, thanks to high energy ion

bombardment during deposition. Hardness results also suggest that the maximum hardness belongs to TiSiN-60, featuring a modified nanocomposite structure. At bias voltages > 60 V, Si content is relatively low, suggesting that nanocomposite formation is less favourable. However, at high bias voltages, the coatings contain a high level of internal stress, and the coating density is significantly higher, which can also contribute to high hardness. The crystallite size study, based on the SR-XRD data, given in Figure 7(a), shows that the TiN crystallite size, in coatings deposited at high bias voltages -70 to -80, is not stable. The relatively rapid crystallite growth in these samples (compared to TiSiN-50 and TiSiN-60V) may result in coating softening due to the annihilation of defects and stress-release at high temperatures. As discussed before, TiO_2 and Ti_2O_3 were observed only in coatings deposited at low bias voltages, while coatings deposited at higher bias voltages (>40V) consist of only cubic (c-) (Ti,Si)N solid solutions. These, as well as the observed porous microstructure, observed in the TiSiN-30V sample, could also be the factors contributing to the lower hardness and elastic modulus for the coatings deposited at lower bias voltages.

In summary, indentation results show an overall trend that the mechanical properties of the coatings, in this study, constantly improved as the bias voltage increases, which could be attributed to: densification of coatings, higher residual stress, less Si content, smoother and more homogeneous surface, and low porosity in the coatings deposited using higher bias voltages. Interestingly, if it is possible to further decrease the crystalline size then the hardness may be further enhanced, but the elastic modulus may be reduced.

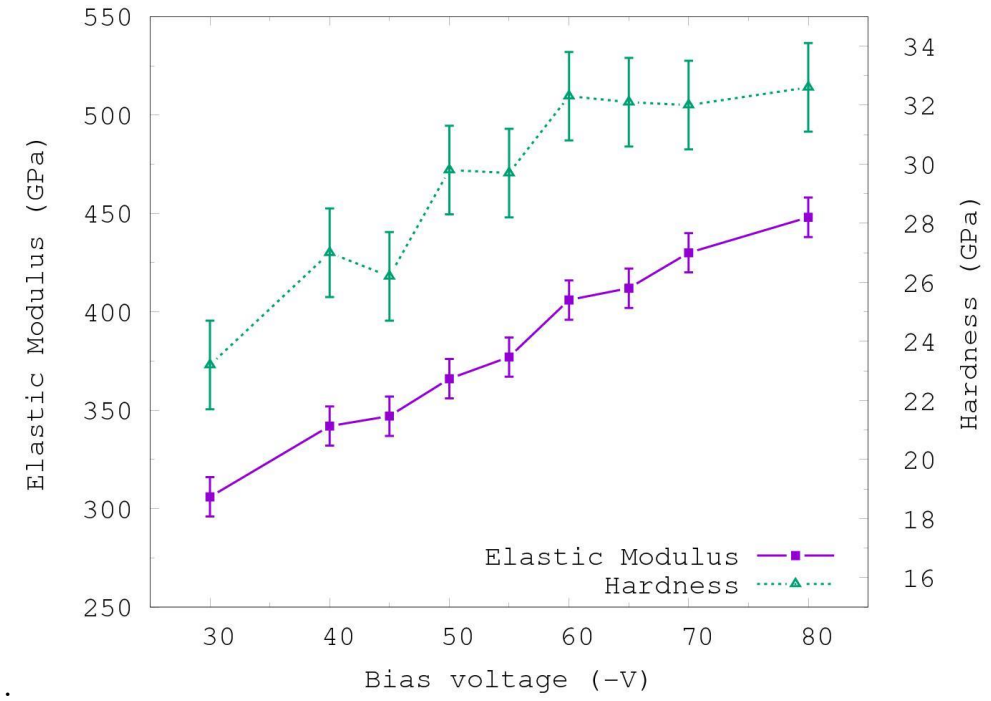

Figure 9. Hardness and Elastic modulus of TiSiN as a function of bias voltage from nanoindentation experiments.

Figure 10 shows the influence of bias voltage and silicon content, on internal stress (σ) embedded in dominant TiN(111) orientation, in TiSiN coatings. These measurements are based on Eq. 1, in which the changes in d-spacing, along TiN(111), in TiSiN coatings (d), deposited at various bias voltages, compared to d-spacing, in the TiN coating (d_0), at each temperature.

$$\sigma = \frac{E}{(1-\nu)} \times \frac{d-d_0}{d_0} \qquad \text{Eq. 1}$$

where E (Elastic modulus) and ν (Poison ratio) are assumed for TiN as 300 GPa and 0.23, respectively. For as-deposited coating, residual stress constantly changes with bias voltage increments from the maximum tensile stress of ~6 GPa in TiSiN-30V to minimum compressive

stress of ~-4 GPa in TiSiN-80V. The compressive residual stresses in the coating film were shown to promote the coating mechanical properties and resist crack propagation [31]. The gradual changes in internal stress from tensile to compressive stresses could be an effective parameter in constant hardness increases in TiSiN coating as shown in Figure 10.

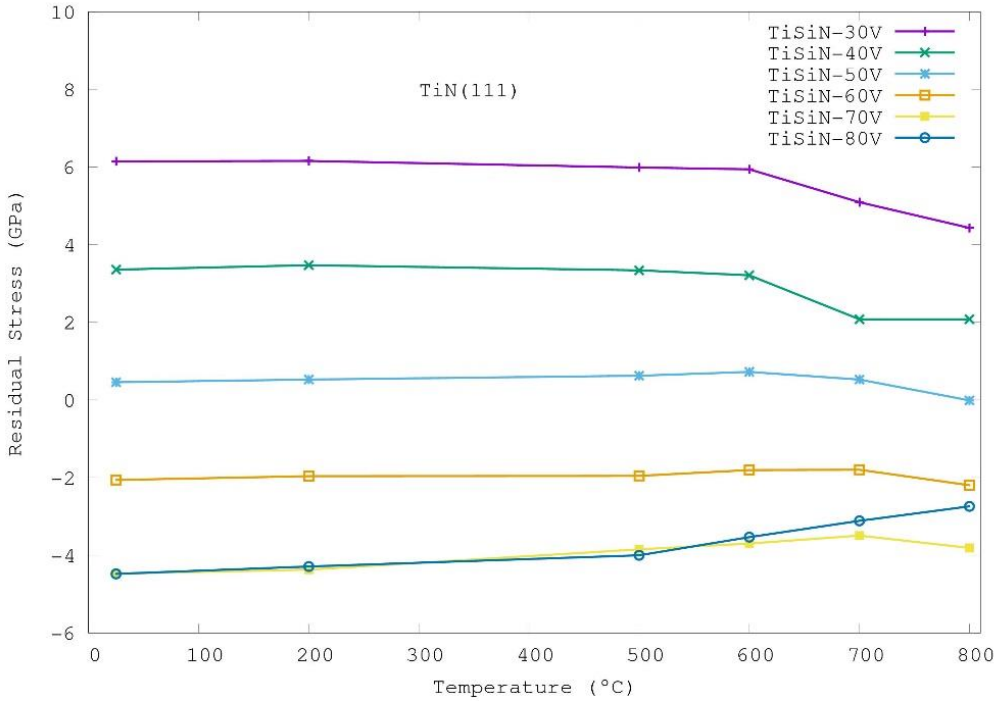

Figure 10. The residual stress, for TiN(111), in TiSiN coatings, as a function of bias voltage, compared to TiN coating, at various temperatures.

It can be seen that the internal stress is strongly sensitive to deposition parameters, such as: chamber pressure and substrate bias voltages/temperature [8],[32]. The residual internal stress, for the TiSiN-50V coating, is close to zero, in as-deposited state, during *in situ* experiment and eventually reaches zero at 800 °C.

Internal stresses are stable up to 600 °C, in TiSiN coatings, and then significantly changes in some of the coatings at temperatures up to 800 °C, which could be due to the microstructure instability at high temperatures. Coatings deposited at bias voltages of -30, -40 and -80V showed various levels of stress-release during the *in situ* experiments above 600 °C, which reveal degrees of ineffective microstructural refinement and nanocomposite formation. Although TiSiN-70V and -80V coating exhibit a high level of compressive stresses, the internal stresses are unstable above 600 °C and may lead to coating softening at high temperatures. TiSiN-60V is the only coating that shows significant hardness, internal compressive stress and stability during the *in situ* test.

4. Conclusions

In the present study, the influence of deposition bias voltage (-30 to -80V) on TiSiN coatings, deposited by magnetron sputtering, was investigated using a number of experimental techniques. Analysis shows that the coatings deposited at bias voltage of -50 V and above produce stable phase composition in the temperature range of 25 to 800 °C, which consists of nc-(Ti,Si)N embedded in a- Si_3N_4, with smooth surface typography and enhanced hardness (33GPa). Higher negative bias voltage significantly changes the phase composition, stability, microstructure and surface morphology of the coatings, which, in turn, resulted in desirable improvement in the oxidation resistance, thermal stability, and mechanical properties. Both the hardness and Young's modulus, of the coatings, constantly improved, from 23 GPa to 33 GPa and 310 GPa to 450 GPa, respectively, as the substrate bias voltage increases from -30 V to -80 V, representing almost 50% increase.

Acknowledgments

Ehsan Mohammadpour is highly grateful to Murdoch University for the scholarship (MIPS) award. This research was undertaken on the powder diffraction beamline at the Australian Synchrotron, Melbourne, Australia (AS141/PD/7582). The study was supported by grants of computing time from the National Computational Infrastructure (NCI), Canberra, Australia, the PAWSEY Supercomputing Centre, Perth, Australia and Ministry of Higher Education, Malaysia (Fundamental Research Grant Scheme FRGS/1/2020/TK0/UMS/02/7). Authors wish to thank Dr Zhi-Feng Zhou for providing sample preparation facility at the City University of Hong Kong.

References

[1] Li S, Deng J, Yan G, Zhang K, Zhang G. Microstructure, mechanical properties and tribological performance of TiSiN-WS2 hard-lubricant coatings. Appl. Surf. Sci 2014;309:209–17.

[2] Arab Pour Yazdi M, Lomello F, Wang J, Sanchette F, Dong Z, White T, et al. Properties of TiSiN coatings deposited by hybrid HiPIMS and pulsed-DC magnetron co-sputtering. Vacuum 2014;109:43–51.

[3] Tian CX, Yang B, Wan Q, Ding H, Hong MQ, Wang RY, et al. Effects of SiH4 flow rate on microstructure and mechanical properties of TiSiN nanocomposite coatings by cathodic arc ion plating. Vacuum 2015;117:12–16.

[4] Veprek S, Veprek-Heijman MGJ. The formation and role of interfaces in superhard nc-MenN/a-Si3N4 nanocomposites. Surf. Coatings Technol 2007;201(13):6064-70.

[5] Li S, Deng J, Qin X, Ji C. Effects of Ti target current on properties of TiSiN coatings. Surf. Eng 2017;33(8):578–584.

[6] Komarov FF, Konstantinov SV, Pilko VV. Formation of nanostructured TiAlN, TiCrN, and TiSiN coatings using reactive magnetron sputtering. J. Frict. Wear 2014;35(3)215–23.

[7] Wo PC, Munroe PR, Zhou ZF, Li KY, Xie ZH. “Effects of TiN sublayers on the response of TiSiN nanocomposite coatings to nanoidentation and scratching contacts. Mater. Sci. Eng. A 2010;527(16–17):4447–57.

[8] Cheng YH, Browne T, Heckerman B, Gannon P, Jiang JC, Meletis EI, et al. Influence of Si content on the structure and internal stress of the nanocomposite TiSiN coatings deposited by large area filtered arc deposition. J. Phys. D. Appl. Phys 2009;42(12)125415.

[9] Choi SR, Park IW, Park JH, Kim KH. Influence of substrate bias voltage on deposition behavior and micro-indentation hardness of Ti-Si-N coatings by a hybrid coating system of arc ion plating and sputtering techniques. Surf. Coatings Technol 2004;179(1)89–94.

[10] Yang ZT, Yang B, Guo LP, Fu DJ. Effect of bias voltage on the structure and hardness of TiSiN composite coatings synthesized by cathodic arc assisted middle-frequency magnetron sputtering. J. Alloys Compd 2009;473(1–2)437–41.

[11] Benegra M, Lamas DG, Fernández de Rapp ME, Mingolo N, Kunrath AO, Souza RM. Residual stresses in titanium nitride thin films deposited by direct current and pulsed direct current unbalanced magnetron sputtering. Thin Solid Films 2006;494:146–50.

[12] Vaz F, Rebouta L, Goudeau P, Girardeau T, Pacaud J, Riviére JP, Traverse A. Structural transitions in hard Si-based TiN coatings: The effect of bias voltage and temperature. *Surf.* Coatings Technol 2001; 146–147:274–79.

[13] Shuangquan R, Jun H, Hongjun W, Canxin T, Liping G, Dejun F. Effects of Bias Voltage on the Structure and Mechanical Properties of Thick CrN Coatings Deposited by Mid-Frequency Magnetron Sputtering. Plasma Sci. Technol 2009;11(1)38–41.

[14] Devia DM, Restrepo-Parra E, Arango PJ, Tschiptschin AP, Velez JM, TiAlN coatings deposited by triode magnetron sputtering varying the bias voltage. Appl. Surf. Sci 2011;257(14):6181–85.

[15] Chu K, Shum PW, Shen YG. Substrate bias effects on mechanical and tribological properties of substitutional solid solution (Ti, Al)N films prepared by reactive magnetron sputtering. Mater. Sci. Eng. B 2006;131(1–3): 62–71.

[16] Hsu C-H, Chen K-L, Lin Z-H, Su C-Y, Lin C-K. Bias effects on the tribological behavior of cathodic arc evaporated CrTiAlN coatings on AISI 304 stainless steel. Thin Solid Films 2010;518(14):3825–29.

[17] Chang C-L, Lin C-T, Tsai P-C, Ho W-Y, Wang D-Y. Influence of bias voltages on the structure and wear properties of TiSiN coating synthesized by cathodic arc plasma evaporation. Thin Solid Films 2008;516(16):5324–29.

[18] Greczynski G, Patscheider J, Lu J, Alling B, Ektarawong A, Jensen J, Petrov I, Greene JE, Hultman L, Control of $Ti_{1-x}Si_xN$ nanostructure *via* tunable metal-ion momentum transfer during HIPIMS/DCMS co-deposition. Surf. Coatings Technol 2015;280:174–84.

[19] Coelho AA, Indexing of powder diffraction patterns by iterative use of singular value decomposition. J. Appl. Crystallogr. 2003;36(1):86–95.

[20] Cheary RW, Coelho AA, and Cline JP. Fundamental parameters line profile fitting in laboratory diffractometers. J. Res. Natl. Inst. Stand. Technol 2004:109(1):1–25.

[21] Gražulis S, Daškevič A, Merkys A, Chateigner D, Lutterotti L, Quirós M, et al. Crystallography Open Database (COD): An open-access collection of crystal structures and platform for world-wide collaboration Nucleic Acids Res 2012;40(D1):420–27.

[22] Toraya H, Huang TC, Wu Y. Intensity enhancement in asymmetric diffraction with parallel-beam synchrotron radiation, J. Appl. Crystallogr 1993;26(6):774–77.

[23] Masson O, Guinebretière R, Dauger A. Reflection Asymmetric Powder Diffraction with Flat-Plate Sample using a Curved Position-Sensitive Detector (INEL CPS 120), J. Appl. Crystallogr1996;29(5):540–46.

[24] Rowles MR, Madsen IC. Whole-pattern profile fitting of powder diffraction data collected in parallel-beam flat-plate asymmetric reflection geometry. J. Appl. Crystallogr 2010;43(3):632–34.

[25] Perdew JP, Wang Y. Accurate and simple analytic representation of the electron-gas correlation energy. Phys. Rev. B 1992;45(23):13244–49.

[26] Kresse G, Hafner J. Ab initio molecular dynamics for liquid metals. Phys. Rev. B 1993;47(1):558–61.

[27] Otero-de-la-Roza A. Luaña V. Gibbs2: A new version of the quasi-harmonic model code. I. Robust treatment of the static data," Comput. Phys. Commun 2011;182(8):1708–20.

[28] Vinett P, Rose JH, Ferrante J,. Smith JR. Universal features of the equation of state of solids from a pseudospinodal hypothesis. Phys. Rev. B 1996;53(9):5252–58.

[29] kadletz M, Schalk N, Daniel R, Keckes J, Czettl C, Mitterer C. Advanced characterisation methods for wear resistant hard coatings: A review on recent progress. Surf. Coatings Technol 2016;285:31–46.

[30] Bartosik M, Holec D, Apel D, Klaus M, Genzel C, Keckes J, et al. Thermal expansion of Ti-Al-N and Cr-Al-N coatings. Scr. Mater 2017;127:182–85.

[31] Musil J, Jirout M, “Toughness of hard nanostructured ceramic thin films. Surf. Coatings Technol 2007;201(9–11):5148–52.

[32] Schalk N, Mitterer C, Keckes J, Penoy M, Michotte C. Influence of residual stresses and grain size on the spinodal decomposition of metastable $Ti_{1-x}Al_xN$ coatings. Surf. Coatings Technol 2012;209:190–96.

Supplementary information

Table S1. *hlk* values for major phases extracted from the in-situ SR-XRD spectra as shown in Figures S1-S7

TiN (•)	~2θ	TiO_2 (♦)	~2θ	Ti_2O_3 (o)	~2θ
(111)	19.24	(110)	14.52	(012)	12.71
(002)	22.26	(011)	18.97	(104)	17.35
(022)	31.68	(020)	20.59	(110)	18.47
(311)	37.34	(111)	21.61	(113)	21.26
(222)	39.06	(210)	23.05	(024)	25.58
(004)	45.42	(211)	28.14	(116)	27.84
(331)	49.76	(220)	29.28	(214)	31.80
(042)	51.14	(002)	32.16		
(422)	56.44	(310)	32.83		
(333)	60.20	(031)	35.13		
(511)	60.20	(112)	35.45		
(044)	66.18	(311)	36.69		
(531)	69.64	(022)	38.49		
(442)	70.77	(212)	39.94		
		(321)	41.06		
		(040)	41.89		
		(330)	44.56		

	(411)	46.36
	(312)	46.62
	(013)	50.30
	(113)	51.48
	(213)	54.91
	(333)	56.01
	(033)	59.27
	(522)	67.46

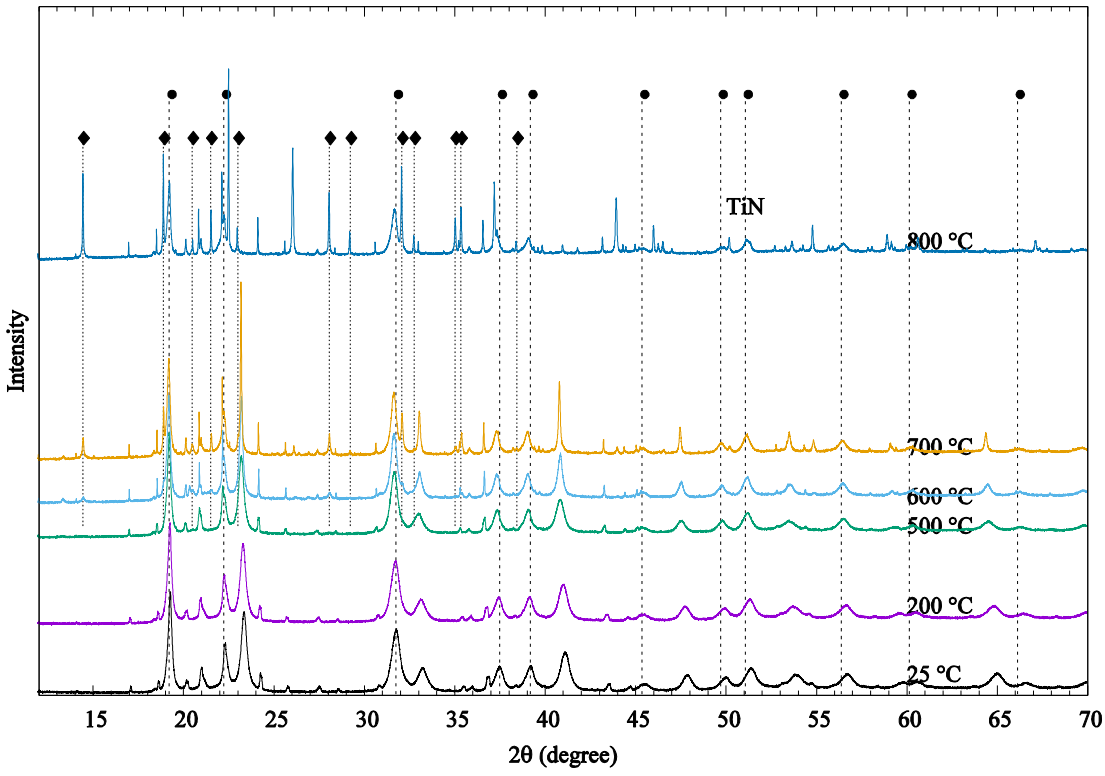

Figure S1. *In situ* SR-XRD data for TiN coating heated from 25 to 800 °C in air

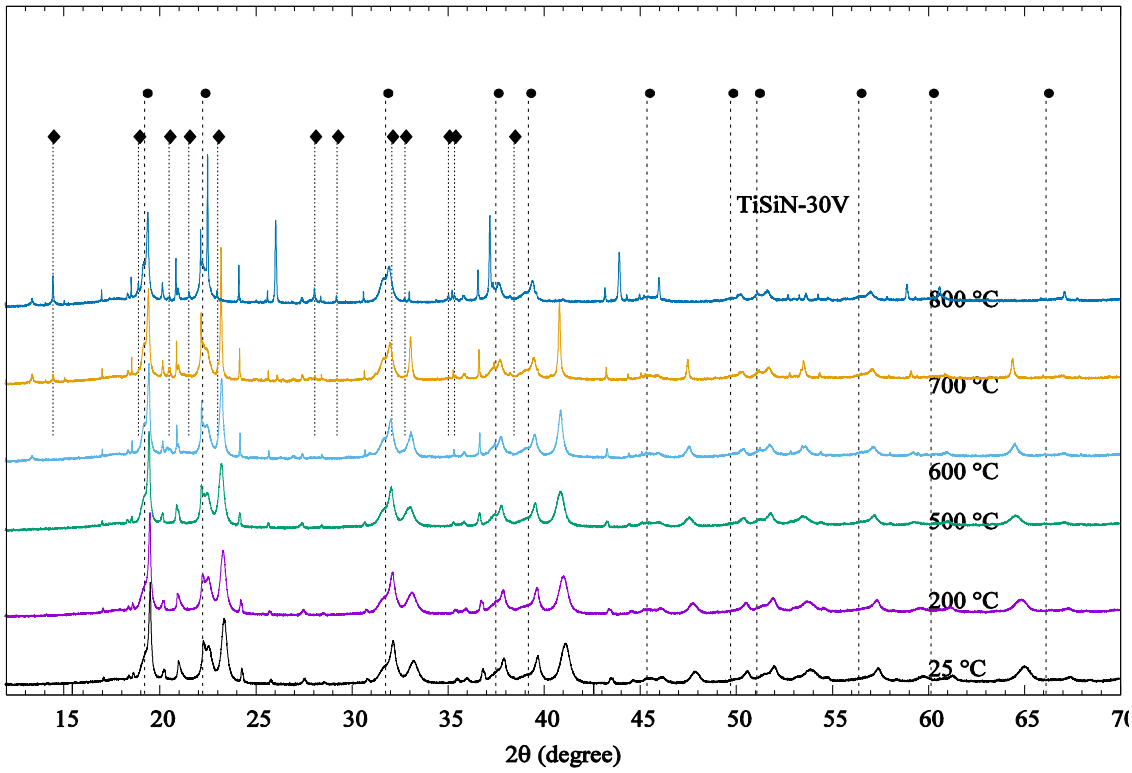

Figure S2. *In situ* SR-XRD data for TiSiN-30 coating heated from 25 to 800 °C in air

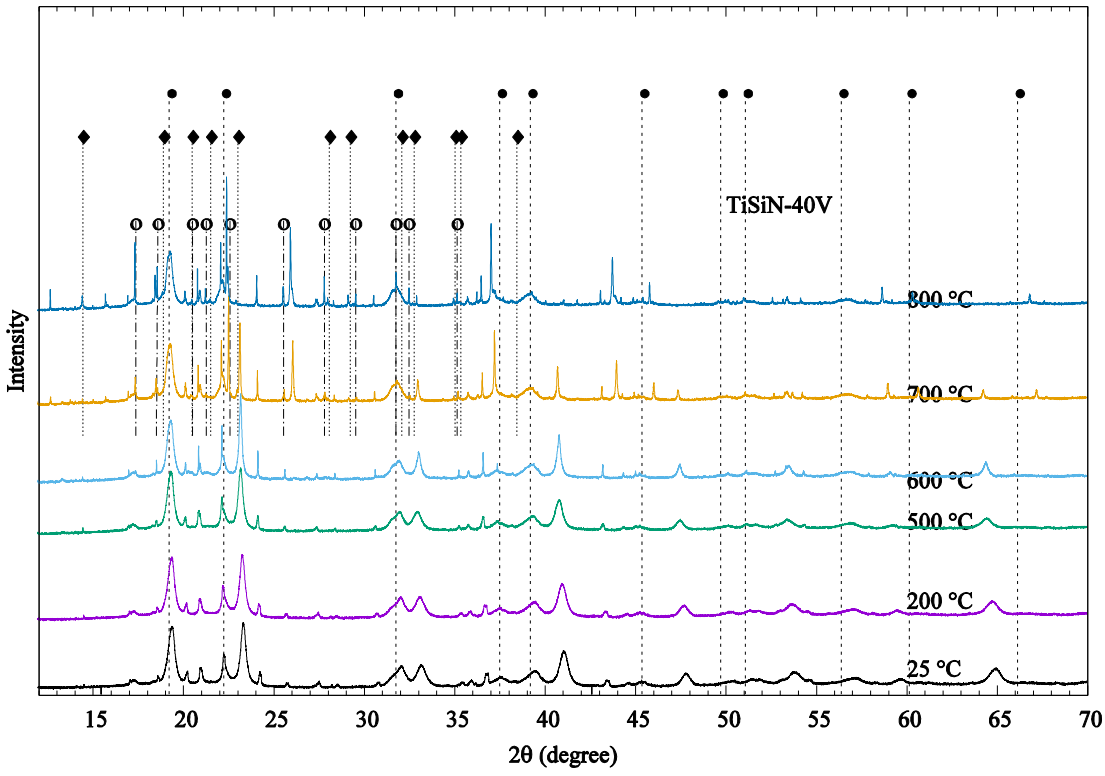

Figure S3. *In situ* SR-XRD data for TiSiN-40 coating heated from 25 to 800 °C in air

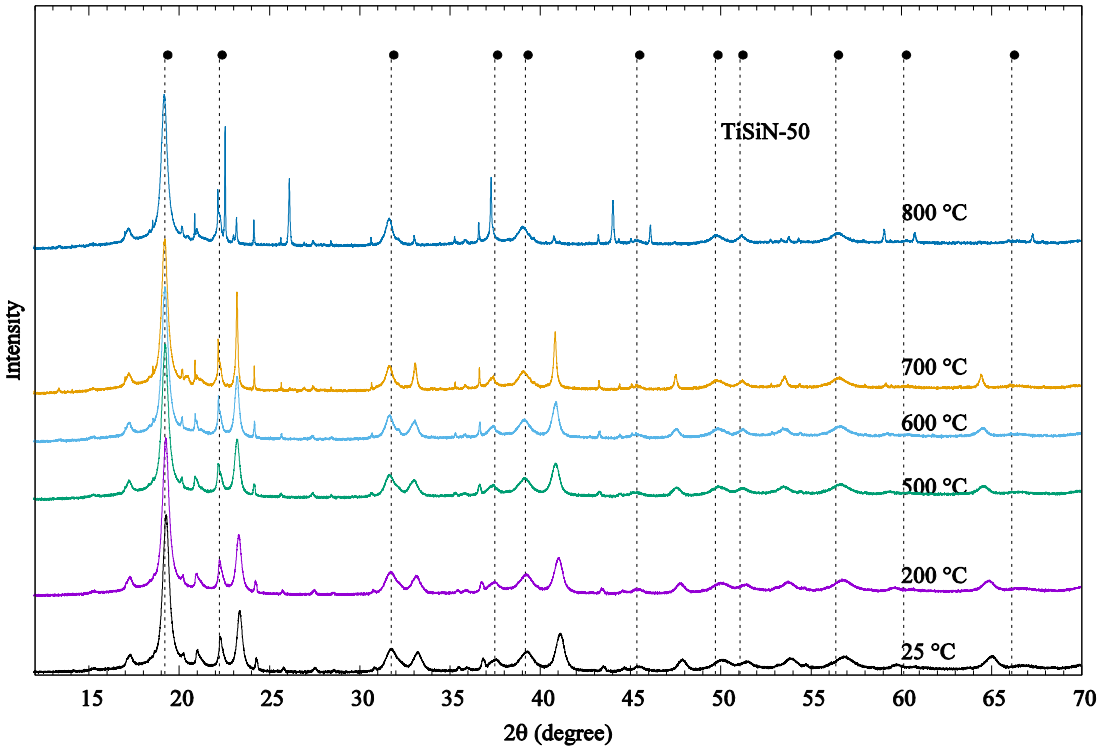

Figure S4. *In situ* SR-XRD data for TiSiN-50 coating heated from 25 to 800 °C in air

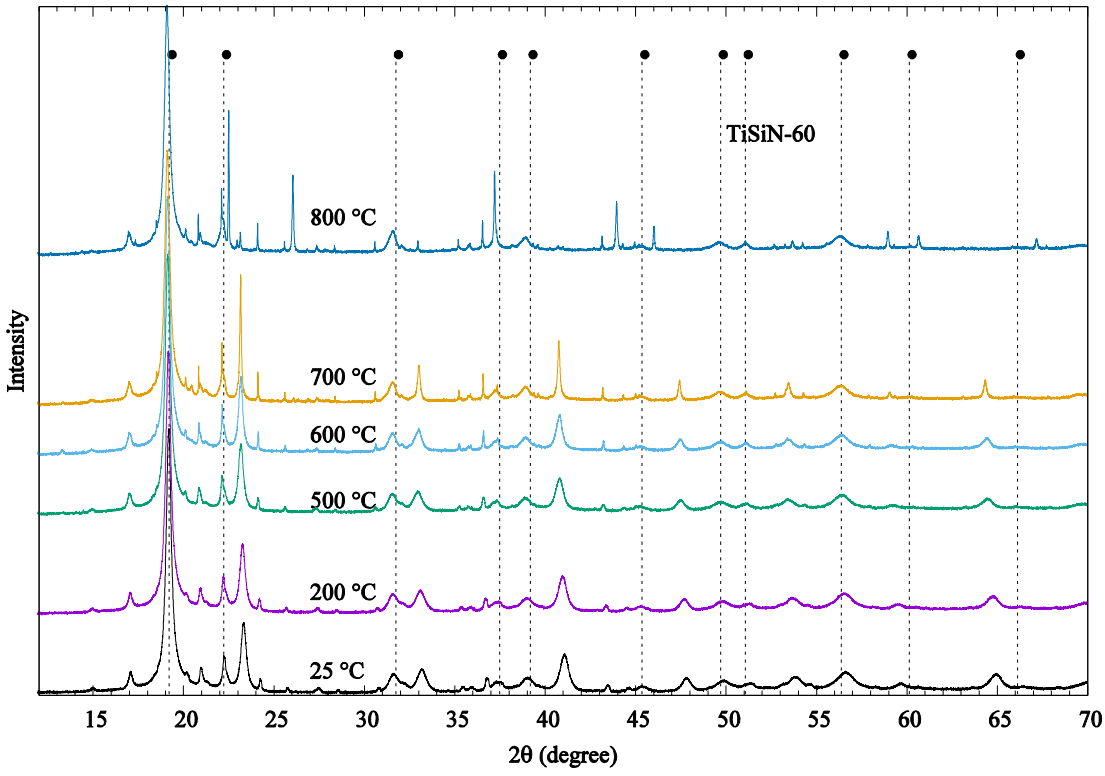

Figure S5. *In situ* SR-XRD data for TiSiN-60 coating heated from 25 to 800 °C in air

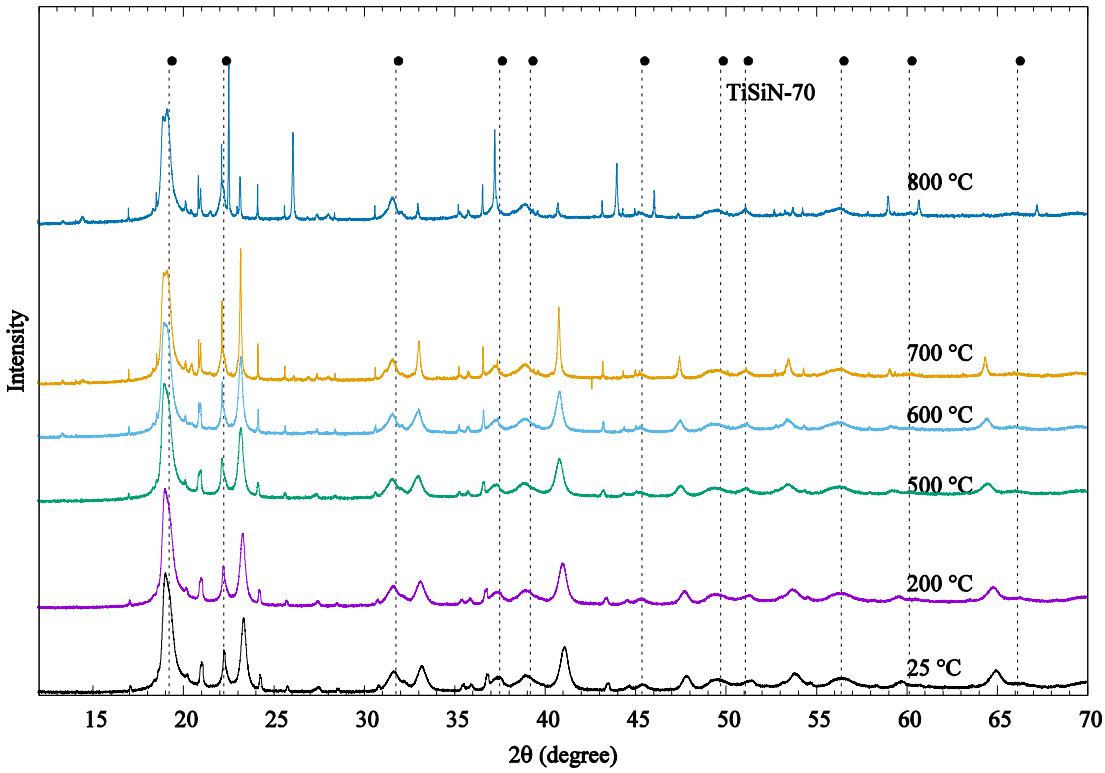

Figure S6. *In situ* SR-XRD data for TiSiN-70 coating heated from 25 to 800 °C in air

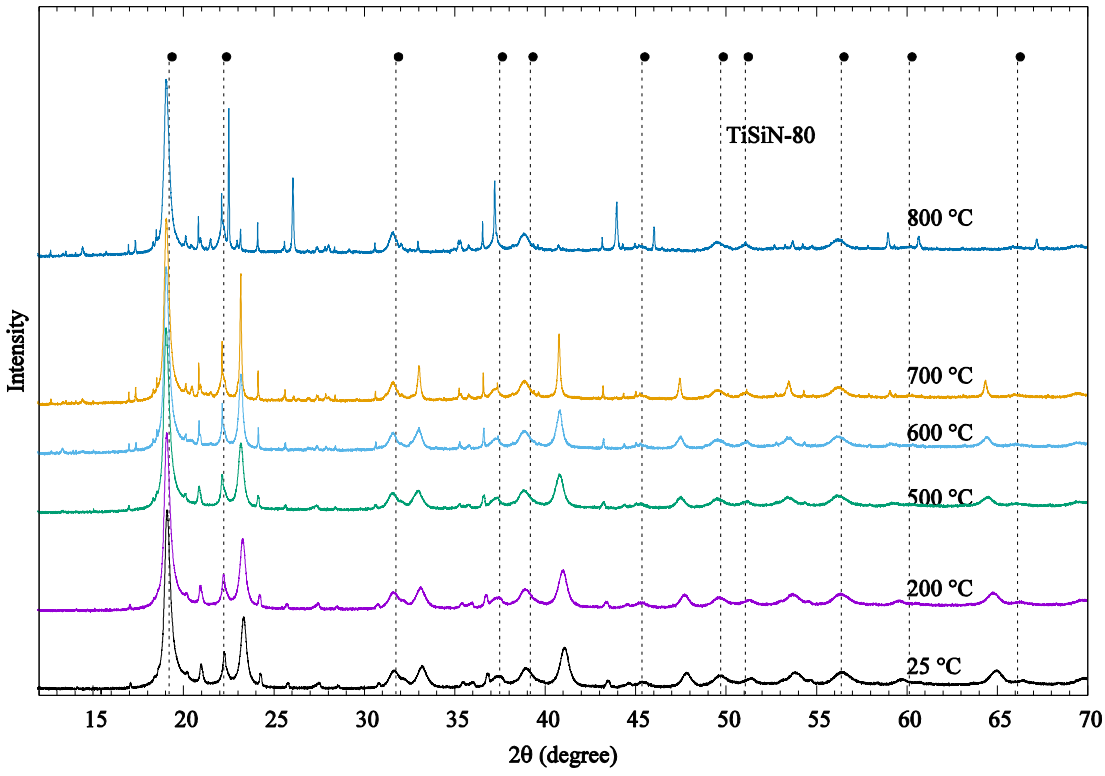

Figure S7. *In situ* SR-XRD data for TiSiN-80 coating heated from 25 to 800 °C in air